Dielectric Modeling of *Staphylococcus Aureus* Bacteria and Shape Optimization of Electrodes for Isolation in Microfluidic Channel: A Numerical Study

Sanchanna Ganesan
Department of Electronics and Instrumentation Engineering, SRM Institute of Science and Technology, Kattankulthur, Tamil Nadu, India
zoneofsanchu@gmail.com (corresponding author)

Juliet. A. Vimala
Department of Electronics and Instrumentation Engineering, SRM Institute of Science and Technology, Kattankulthur, Tamil Nadu, India
vimalaja@srmist.edu.in

C. Likith Kumar
Department of Electronics and Instrumentation Engineering, SRM Institute of Science and Technology, Kattankulthur, Tamil Nadu, India
likith.chinnapalli@gmail.com

Received: 15 June 2024 | Revised: 9 July 2024, 16 July 2024, and 23 July 2024 | Accepted: 30 July 2024

 DOI: https://doi.org/10.48084/etasr.8144

ABSTRACT

This study investigates the optimization of the electrode shape to isolate bacteria from the blood within a microfluidic channel, employing the dielectrophoretic technique. The examination focuses on the dielectric modeling of *Staphylococcus Aureus* bacteria to isolate them from blood components, specifically Red Blood Cells (RBC) and platelets. The numerical study utilized the COMSOL Multiphysics software to model three distinct channels, using standard geometric shapes such as triangles, rectangles, and circles as their electrodes. Numerical analyses were carried out to compare the three models and acquire an appropriate electrode configuration to separate *Staphylococcus Aureus* from blood particles. Simulations were carried out for all three models by modifying the voltages and inlet velocities to obtain their efficiency. The results showed that the circular and triangular-shaped electrode models required a low voltage of 4 V to achieve the desired separation of bacteria from blood particles, RBC, and platelets. In contrast, the rectangular-shaped electrode required a higher voltage of 8 V.

Keywords-numerical analysis; electrode optimization; COMSOL multiphysics; staphylococcus aureus

I. INTRODUCTION

A. Dielectrophoresis (DEP)

Microfluidic devices for rapid diagnosis have become essential in identifying or detecting diseases in the biomedical, biotechnology, drug delivery, and point-of-care fields. In recent years, DEP has evolved into one of the promising platforms for medical and diagnostic applications. Drug delivery [1-2], fractional process of gene vaccine [3], detection of cancer cells [4], separation of bioparticles [5] and non-bioparticles [6], sorting of DNA [7], RNA [8], proteins [9] and stem cells [10] quantitative analysis [11], cell characterization [10], etc. are applications involving DEP technology. DEP occurs when an inhomogeneous electric field (AC and DC) is given to a particle and its medium, causing the particle to move in a direction different from the electric field due to its varying polarizability. The result varies based on the permittivity, dimension, and conductivity of the cell as well as the medium. The force on the particle is given by

$$F_{DEP} = 2\pi e_m r^3 RE\{F_{CM}\}\nabla E_{rms}^2 \quad (1)$$

where ε_m is the permittivity of the medium, r is the particle radius, E_{rms} is the mean square root of the applied electric field, and $RE\{F_{CM}\}$ is the real value of the Clausius - Mossotti Factor (CM).

$$F_{CM} = \frac{\varepsilon Cell^* - e_m^*}{\varepsilon Cell^* + 2e_m^*} \quad (2)$$

where $\varepsilon Cell^*$ is the complex permittivity of the cells, and ε_m^* is the complex permittivity of the medium.

$$\varepsilon^* = \varepsilon - j\frac{\sigma}{\omega} \quad (3)$$

where ε is permittivity, σ is conductivity, j is the imaginary unit, and ω is the angular frequency.

The phenomenon known as positive DEP (p-DEP) occurs when particles exhibit greater polarizability than the medium and migrate toward the region of higher electric potential. In contrast, particles moving toward lower concentration encounter negative DEP forces. The particles exhibit forces that are influenced by their dielectric properties and the frequency of the applied field that is given to the electrodes. The relationship between the dielectrophoretic force and the square of the applied electric field is shown in (1).

B. Literature Review

In [12, 13], extensive reviews of theory, technology, and applications showed how DEP was technically established as a research field. Despite these technical advancements and research, few practical areas are under the development stage and focus of study. One such area in DEP applications is designing and optimizing the electrode design for the microfluidic chip in isolation or separation for micron and sub-micron particles. DEP forces depend on the nonuniform electric field, which is determined by the electrode shape, size, and geometry. The electric field can be altered to generate a non-uniform electric field by optimizing the electrodes' geometry (shape, size) and arrangement (gaps, angle, and number of electrodes). Electrode geometry is the key factor, as it decides the required DEP force needed and other parameters, such as the temperature inside the device that affects cell physiology, such as membrane disruption, damage to the cell, and other electro-physiological effects generated in the suspended medium. Different types of electrode configurations have been reported in the literature. In [14], the separation of g-iDEP serotypes of Escherichia coli was reported and validated experimentally, proving a gradient-based insulator.

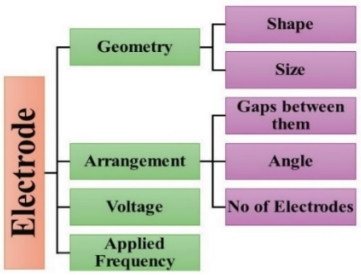

Fig. 1. Parameters for electrode optimization.

DEP is used for separatory and diagnostic applications. Interdigitated electrode array configurations have been used to quantitatively characterize the mechanical properties of biological cells. In [15], a device with interdigitated electrodes was proposed to characterize healthy and affected human Red Blood Cells (RBCs) by identifying their biophysical properties using the DEP method. In [16], electrodeless DEP (E-DEP) was presented to isolate single- and double-stranded DNA. Circular electrodes are preferably used for particle separation using DEP. C. L. Shing developed an innovative device that provides a separation solution with a low sample volume of 50 nl using DEP and Circular Traveling Wave Electroosmosis (TWEO) methods [17]. In [18], microarray dot gold electrodes were manufactured for size-based separation and experimentally validated by separating 1 μm, 5 μm, and 15 μm polystyrene particles. In [19], sorting and streaming of stem cells from SC23 to SC27 was performed using circle, diamond, and lens-shaped arrays with 10%, 50%, and 100% channel height, respectively, along with numerical analysis to determine the device's efficiency. In [20], separation and manipulation of LNCaP prostate cancer in the form HCT116 was performed with colorectal cancer cells using a thin film electrode arranged 45° from the main channel, studying the separation and enrichment factors. In [21], a trapezoidal electrode array, with metallic legs measuring 120 μm longer base, 20 μm shorter base, and 60 μm height, was used to separate polystyrene microparticles. In [22], numerical modeling was carried out to separate CTC and WBC for MCF-7 cells, using four hyperbolic-shaped electrodes arranged coherently to the walls. In [23], a numerical simulation-based performance improvement of DEP was presented to separate circulating tumor cells from the bloodstream in a microfluidic platform using slanted and interdigitated planar electrodes. In [8], circular, triangular, and rectangular obstacles with side wall electrodes were used to separate CTC (MDA-MB231) from RBC, with rectangular obstacles having a higher non-uniformity of the electric field when voltage was set to 6V, achieving 100% separation and purity of cancerous cells at specific outlets.

C. Scope of this Study

This study aims to numerically optimize the shape of the electrodes using the DEP technique to isolate *Staphylococcus Aureus* (staphylococcus), which is one of the potentially fatal bacteria that cause sepsis [24], from blood components such as RBCs and platelets in a microfluidic channel. COMSOL Multiphysics software was used to design and simulate three electrodes of distinct shapes, placed on the sidewalls of the microfluidic channels. Each channel consists of triangle-, rectangle-, and circle-shaped electrodes arranged in equal intervals. Before simulation, mathematical single-shell modeling was established to identify the global parameters of staphylococcus bacteria. During the simulation, uniform dimensions and parameters were used for all three models to determine their selective voltage in the isolation of bacteria. Finally, the performance of these models was analyzed and compared.

II. PROPOSED MODEL

A. Geometry

Figure 2 shows the diagrams of the three microfluidic channel models. The channel geometry includes two inlets, with seven electrodes positioned on the channel's sidewall, and three outlets. The first model includes equilateral triangular-

shaped electrodes with a base and a height of 40 μm. The second model features rectangular-shaped electrodes with height and width of 40 μm each. The third model has circular-shaped electrodes with a diameter of 40 μm. A nonuniform electric field with alternating polarity is created to achieve particle separation. The inlet-I is intended to suspend particles, while the buffer medium is suspended in inlet-II. Both inlets are 40 μm in width and 200 μm in height and are connected to the main channel at a 45° angle. The primary channel is constructed with a width of 560 μm and a height of 40 μm, containing seven electrodes positioned with a 40 μm gap between each other in the three models. The outlets are constructed with a width of 40 μm and a height of 200 μm, positioned at a distance of -450 and +450 from one other respective to the channel. The material used for channel geometry was PDMS. The finite element analysis method was adopted to solve the CFD problem [25]. The simulation analysis of the channel's modeling and design was carried out using COMSOL Multiphysics v6.2 FEM software. A system equipped with an Intel i7 CPU, 16 GB of RAM, and a 64-bit operating system was used to carry out the simulations.

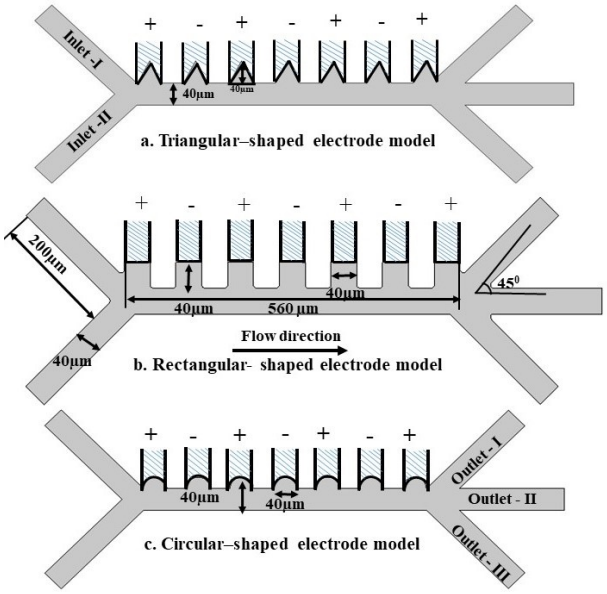

Fig. 2. Three distinct computational channels with different electrode shapes.

B. Dielectric Modelling

Staphylococcus is a minuscule organism that falls under the category of gram-positive bacteria. A bacterial cell has a spherical shape and is composed of three layers: the inner, which contains the plasma and nucleus, the middle, known as the cytoplasm, which is surrounded by the cell membrane, and the outer, which is the wall membrane. The middle membrane of gram-positive bacteria is a thick cell wall layer that has a size of 20-80 nm. When converted to the dielectric model, each shell has distinct electrical properties and varying radii consolidated into a single-cell membrane with equal conductivity and permittivity, as shown in Figure 3. The measurement of the cell radius (R) involves the measurement of the distance between the central region of the inner membrane, encompassing the plasma and nucleus, and the outer wall membrane. Figure 3 shows the bacterial equivalent modeling and Figure 4 illustrates the actual component of the CM factor, which represents the particles' operating frequency.

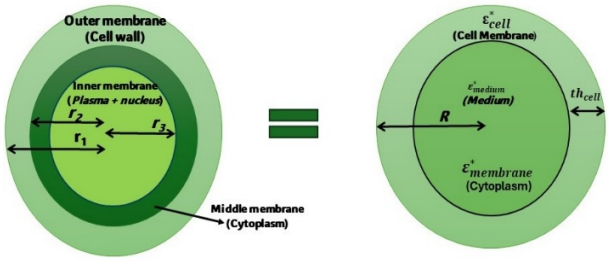

Fig. 3. Single shell modeling of the Staphylococcus bacteria.

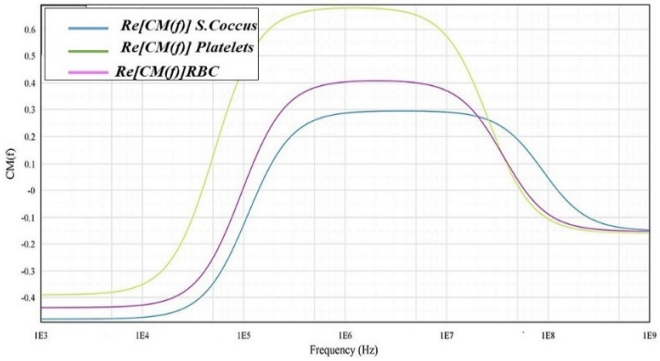

Fig. 4. Real part of the CM factor of the particles.

The equivalent modeling of the cell is given by [26]:

$$\varepsilon^*_{eq} \quad \varepsilon^*_s \frac{(\frac{r_o}{r_i})^3 + 2\frac{(\varepsilon^*_p - \varepsilon^*_s)}{\varepsilon^*_p + 2\varepsilon^*_s}}{(\frac{r_o}{r_i})^3 - 2\frac{(\varepsilon^*_p - \varepsilon^*_s)}{\varepsilon^*_p + 2\varepsilon^*_s}} \tag{4}$$

where r_0 and r_i are the outer and inner radii of the shell, respectively, ε_p is the complex permittivity of the particles, and ε_s is the complex permittivity of the outer shell. Calculating the DEP forces involves substituting the complex permittivity of the particle with the equivalent complex permittivity of a uniform particle, considering the shell and internal compounds of the particle. The DEP force is proportional to particle size, the applied frequency, and the square of the applied electric field. Staphylococcus has a diameter of 1 μm, density of 1000 kg/m^3, conductivity of 0.75 S/m, and a relative permittivity of 66, as given in [27]. Similarly, the particle properties of RBC and platelets were taken from [28]. From the graph of the CM factor and frequency, it is evident that the staphylococcus bacteria exhibit positive DEP at 10 KHz frequency, and RBCs exert a greater DEP energy due to their larger radius. Compared to platelets and staphylococcus, RBCs move further away and are collected at distinct outlets. The larger RBC particles are displaced further away from the first streamline, resulting in a third outlet. Secondly, the platelets move a smaller distance from the streamline to outlet-II, and finally, the staphylococcus bacteria get collected on outlet-I.

C. Modeling and Simulation

The proposed model was developed in COMSOL Multiphysics. Figure 5 shows the steps followed in the simulation.

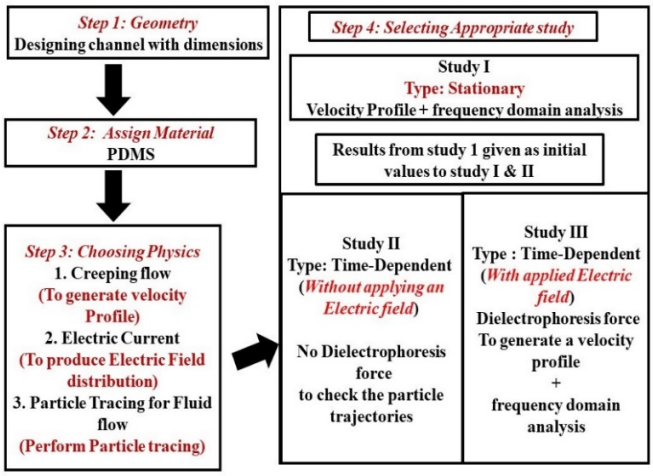

Fig. 5. Steps followed in simulation.

The initial step was to design the geometrical part with the necessary dimensions. Secondly, polydimethylsiloxane (PDMS) was chosen as the material. The next step was to choose the physics used in the model. The simulation involves the coupling of three physics modules: AC/DC, particle tracing module, and creeping flow module. The flow of the fluid in the main channel is determined using the creeping flow module, while the electric field distribution is calculated using the AC/DC module. The particle trajectory tracing module calculates particle streamlines in the channel, taking into account the combined effects of fluid flow and electric field on the particle's path. The velocity profile in creeping flow is determined using the principles of continuity and the Navier-Stokes equation. The fluid has a Reynolds number of less than one and is assumed to be incompressible in this model. The equations below are COMSOL Multiphysics-generated equations that can be solved using the Finite Element Method (FEM) for this model.

$$\rho\left(\frac{\partial u}{\partial t}+u.\nabla u\right)=-\nabla p+\nabla.\left(\mu(\nabla u+(\nabla u)^{T})-\frac{2}{3\mu(\nabla.u)I}\right)+F_{gravity} \quad (5)$$

The external force is insignificant due to the cells' minimal gravitational effect. Furthermore, the fluid flow is considered incompressible and creeping in nature, implying that the individual streamlines of the cells are generated without mixing. Thus, (5) is transformed as:

$$-(\nabla p)+\nabla.(\mu(\nabla u+(\nabla u)^{T}=0 \quad (6)$$

When normal inflow was considered, both inlet-I and inlet-II had a higher velocity to focus the particle on a single streamline. The outlet's boundary condition of atmospheric pressure was met (P = 0), while the channel side wall had no-slip boundary conditions. The electric field distribution was generated using the AC/DC module inside the channel and is given by the Laplace transform equation as:

$$V.J=Q_i \text{ where } J=\sigma E+J_e \quad E=-V\,V \quad (7)$$

The following are the default assumptions made when running the AC/DC module: the electrodes are initially given an electric potential of 0 V with initial boundary conditions. The channel walls, inlet, and outlet are insulating, so the applied potential on the electrode remains constant. The walls are given a reference impedance of 50 Ω. The particle tracing module is used to track particles. The channel's medium has a conductivity of 0.005 S/m, a relative permittivity of 80, and a density of 1000 kg/m^3. There are four types of forces experienced by particles: dielectrophoretic (DEP), gravitational, mass-induced, and basset forces. Because the particles are in the micron range, the effects of gravity, mass, and basset forces are ignored. The particles experience two forces: F_{DEP}, as described in (1), and F_{drag}, which is given by

$$F_{drag}=-6\pi\mu Rv \quad (8)$$

These are the primary forces acting on the particles in the microchannel. Hydrodynamic flow behavior causes drag forces in the microchannel, which act along its length. On the other hand, Field-induced DEP (FDEP) is caused by the non-uniform electric field generated by the applied potentials to the electrode and acts along the microchannel's width. Drag and DEP forces act perpendicularly to each particle. Finally, three studies were chosen for the entire simulation, with stationary study 1 determining the velocity profile and electric field strength. The findings of the first study serve as the foundation for the second and third studies. A time-dependent study was chosen for studies II and III to obtain the no-DEP force and particle trajectories.

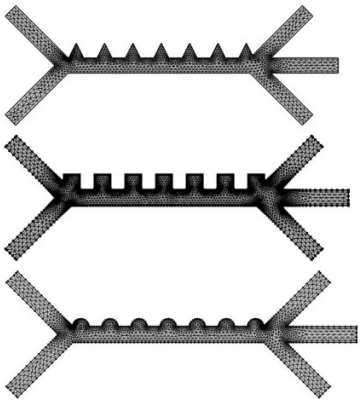

Fig. 6. The meshing of the three models.

D. Mesh Analysis

The simulation for all three models uses a normal elemental size with a physics-controlled sequencing mesh. After simulation, the circular electrode model has 3577 domain elements and 406 boundary elements, the rectangular electrode model has 8470 domain elements and 686 boundary elements, and the triangle electrode model has 2837 domain elements and 389 boundary elements. The variations in the meshing

components arise from the differences in the shape, edges, pointed tip, and grooves of the electrode geometry, as shown in Figure 6.

III. RESULTS AND DISCUSSION

A. Velocity Profile and Focusing Width

Fluid flow velocity is an essential variable to determine the appropriate particle separation in the microchannel. To achieve it, focusing particles are released from their initial positions with a consistent flow of velocity, before entering the region of separation. To achieve optimal focusing, the particles are suspended from inlet-I, while the buffer solution from inlet II is at a higher velocity compared to inlet-I. Figure 7 shows the velocity profile of the three models with the streamlines. The process of particle focusing within the microchannel pertains to the manipulation of particle positions within a single streamline. Simulation was carried out for the three models and the focusing width was obtained by simulating with different inlet velocity ratios. Maximum focus width was achieved with a velocity ratio of 1:6 and resulted in the formation of distinct streamlines, which effectively separate the staphylococcus in outlet-I from platelets and RBCs that are recovered at outlet-II and III, respectively. Further increasing the velocity ratio can achieve greater focus. However, this leads to obstruction of particle motion. The highest focusing width was observed in the rectangular model with 56.2 µm, followed by the circular electrode model with 48.9 µm, and last in the triangular electrode model with 40 µm, as shown in Figure 7.

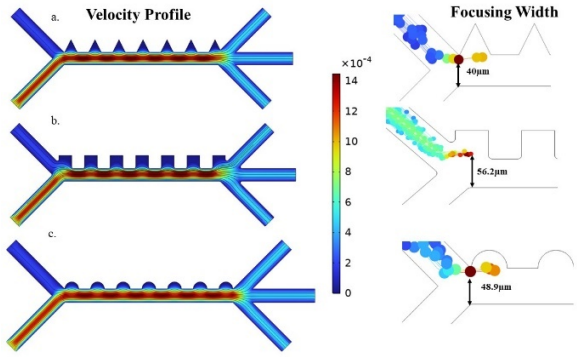

Fig. 7. Velocity profile for the three models and focusing width.

B. Influence of Electrode Geometry on Electric Field Strength

The generation of this non-uniform electric field was achieved by applying a voltage from one peak to another on the electrodes. The geometrical shape of the electrode is crucial in producing the necessary intensity of the non-uniform electric field. The isolation of staphylococcus bacteria according to their dimensions and subsequent separation from blood particles requires a greater magnitude of the DEP force. This typically entails the generation of a high-intensity, non-uniform electric field within the channel. Figure 8 shows the electric field intensity of the three models. The influence of the electric field strength has an impact on the particles as they move through the channel. To investigate the electric field strength, a common distance of the electrode was chosen in the middle of the channel, and the graph was generated for electric field strength and arc length. From Figure 9, it is evident that the circular electrode had a higher electric field strength, followed by the triangular and rectangular electrodes for the same applied voltage of 4 V and 10 KHz frequency.

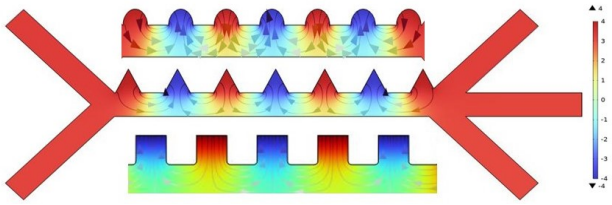

Fig. 8. The Electric potential for the three models for applied 4 V.

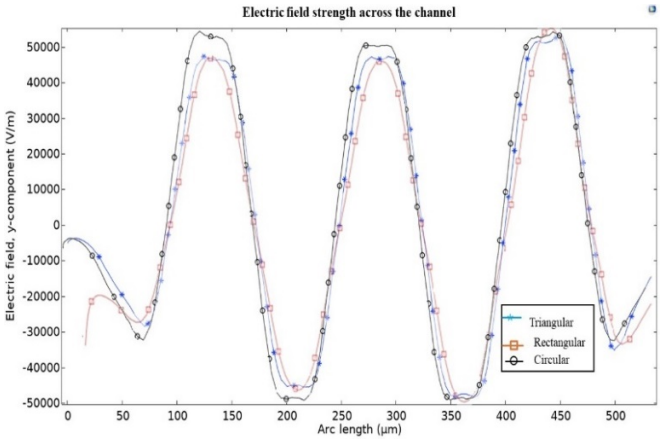

Fig. 9. Electric field strength vs arc length.

C. Influence of Applied Voltage on Separation

Voltage excitation is an essential variable, as it generates heat within the channel, resulting in an increase in temperature that affects the particles. This investigation examines the efficient segregation of three particles across a voltage range of 0 to 10 V, while maintaining inlet velocities of 135 µm S^{-1} and 810 µm S^{-1}, and a working frequency of 10 KHz for the three models. In the absence of an electric field, the particles tend to move toward the first outlet in all three models, as shown in Figure 10. In a triangular electrode, on applying 2 V, staphylococcus and platelets move to the same outlet-I and RBCs to outlet-II. Upon increasing to 3 V, the streamlines were not prominent. At 4 V, proper trajectories of the bacteria were obtained, leading them to outlet-I, platelets to outlet-II, and RBCs to outlet-III. Increasing the voltage to 5 V, the separation took place, with RBCs being stuck it the middle of the channel, as shown in Figure 11.

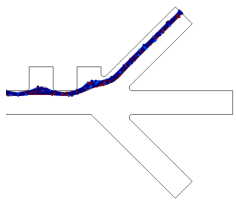

Fig. 10. Without electric field.

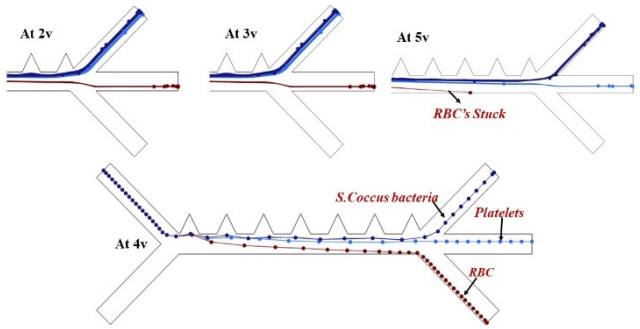

Fig. 11. Separation of the particles at different voltages for the triangular model.

In practice, the RBC particles are suppressed and stuck in the middle, hindering the flow along the channel, which reduces the separation efficiency. By identifying the optimized voltage for the given geometry, this can be avoided. Similarly, for the circular electrode at 2 V, the staphylococcus bacteria and platelets were leading to outlet-I, whereas RBCs were collected at outlet-II. At 3 V, the streamlines of platelets were partial at outlets I and II, however, RBCs were collected at outlet III and staphylococcus bacteria at outlet-I, as shown in Figure 12. At 4 V, the prominent streamlines were obtained by collecting bacteria at outlet-I, platelets at outlet-II, and RBCs at outlet-III. Increasing the voltage to 5 V, RBCs, due to their larger size, become stuck in the middle of the channel.

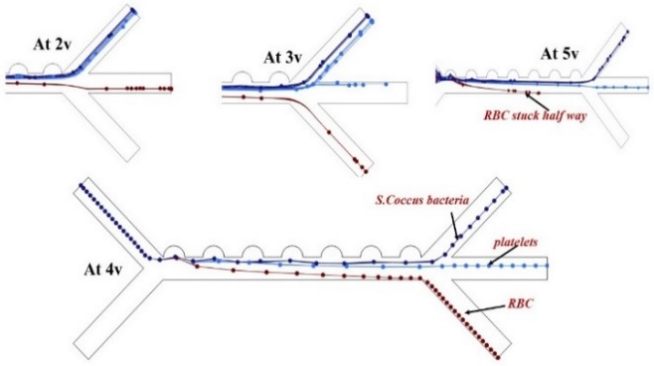

Fig. 12. Separation of the particles at different voltages for the circular model.

Figure 13 shows that at 3 V voltage in the rectangular electrode model, RBCs were initially separated and collected in outlet II. However, both platelets and staphylococcus were separated and collected from the same outlet. At 5 V, platelets and staphylococcus separated partially but continued to accumulate at the same outlet I. Furthermore, elevated voltage caused a limited number of RBC particles to migrate towards outlet III, resulting in partial separation from both outlets II and III. At both voltages, the particles were divided into three distinct groups at the intended outlet. At 8 V, the platelets separated significantly, as evidenced by distinct streamlines.

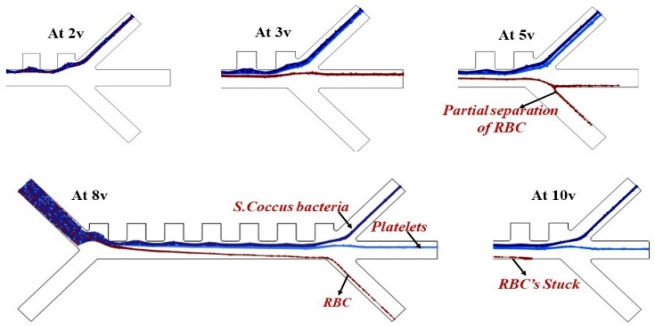

Fig. 13. Separation of particles at different voltages for the rectangular model.

D. Model Performance

To evaluate the performance, a total number of 300 particles were released and simulation was performed for all three models. The graph below shows the number of particles collected at the outlets of the triangular-shaped model with different voltages.

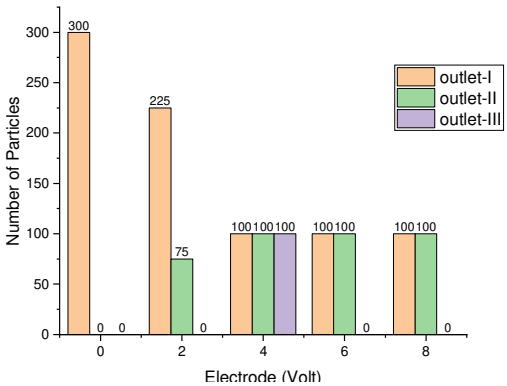

Fig. 14. Number of particles collected at the outlets for different voltages.

In the absence of an electric field, the separation process does not occur, and all particles (300) are collected at outlet-I. However, at 2 V, both platelets and RBC particles are collected along with staphylococcus at outlet-I counting to 225. Similarly, in outlet-II, a mixture of platelets and RBC particles is collected (75), showing partial separation. Increasing the voltage to 4 V, particles are separated at their intended outlets (staphylococcus, platelets, and RBCs at I, II, and III, respectively), indicating complete separation and showing that this is the optimal voltage for this model. Further increasing the voltage to 6 V, the separation of staphylococcus bacteria and platelets occurred at respective outlets I and II, however, the RBCs due to their large size adhered to the side channel walls leading to zero particles at outlet-III. Similarly, for the circular model at 4 V, the particles were separated at their intended outlets counting to 100 each. In the rectangular model, a slight deviation occurred and the complete separation of the particles occurred at 8 V.

IV. CONCLUSION

An extensive numerical study was carried out to evaluate the impact of many factors, such as focusing width, electric

field intensity, and applied voltages, on optimizing the electrode shape to separate staphylococcus bacteria from the blood. The significance of this study lies in the three distinct models, each featuring electrodes shaped like rectangles, triangles, and circles, that are placed in the side walls of the microfluidic channel. A single-shell bacterial modeling framework was established, and the corresponding permittivity and conductivity of the bacterial parameters were identified and incorporated into the model. The rectangular electrode had a focusing width of 56.2 μm, which is greater than that of the circular (48.9 μm) and triangular (40 μm) models. The findings suggest that the circular and triangular models exhibit a unique ability to effectively isolate staphylococcus bacteria from other blood particles with a low voltage of 4 V, resulting in 100% separation. On the other hand, the rectangular electrode model successfully separates bacteria at a higher voltage of 8 V. In the future, the investigated models can be fabricated and experimentally validated with optimal voltages.

ACKNOWLEDGEMENT

The authors express their gratitude to the National MEMS Design Center, the Department of Electronics and Instrumentation Department, SRM Institute of Science and Technology, for providing the lab and computational facilities for executing this work.

REFERENCES

[1] R. Pethig, "Dielectrophoresis: An assessment of its potential to aid the research and practice of drug discovery and delivery," *Advanced Drug Delivery Reviews*, vol. 65, no. 11, pp. 1589–1599, Nov. 2013, https://doi.org/10.1016/j.addr.2013.09.003.

[2] S. M. Patil, S. S. Sawant, and N. K. Kunda, "Exosomes as drug delivery systems: A brief overview and progress update," *European Journal of Pharmaceutics and Biopharmaceutics*, vol. 154, pp. 259–269, Sep. 2020, https://doi.org/10.1016/j.ejpb.2020.07.026.

[3] J. Zhai, W. Gao, L. Zhao, and C. Lu, "Integrated transcriptomic and quantitative proteomic analysis identifies potential RNA sensors that respond to the Ag85A DNA vaccine," *Microbial Pathogenesis*, vol. 149, Dec. 2020, Art. no. 104487, https://doi.org/10.1016/j.micpath.2020.104487.

[4] G. I. Russo *et al.*, "The Role of Dielectrophoresis for Cancer Diagnosis and Prognosis," *Cancers*, vol. 14, no. 1, Jan. 2022, Art. no. 198, https://doi.org/10.3390/cancers14010198.

[5] G. R. Pesch and F. Du, "A review of dielectrophoretic separation and classification of non-biological particles," *Electrophoresis*, vol. 42, no. 1–2, pp. 134–152, 2021, https://doi.org/10.1002/elps.202000137.

[6] F. D. Gudagunti, L. Velmanickam, D. Nawarathna, and I. T. Lima, "Nucleotide Identification in DNA Using Dielectrophoresis Spectroscopy," *Micromachines*, vol. 11, no. 1, Jan. 2020, Art. no. 39, https://doi.org/10.3390/mi11010039.

[7] M. A. Witek, I. M. Freed, and S. A. Soper, "Cell Separations and Sorting," *Analytical Chemistry*, vol. 92, no. 1, pp. 105–131, Jan. 2020, https://doi.org/10.1021/acs.analchem.9b05357.

[8] V. Varmazyari, H. Habibiyan, H. Ghafoorifard, M. Ebrahimi, and S. Ghafouri-Fard, "A dielectrophoresis-based microfluidic system having double-sided optimized 3D electrodes for label-free cancer cell separation with preserving cell viability," *Scientific Reports*, vol. 12, no. 1, Jul. 2022, Art. no. 12100, https://doi.org/10.1038/s41598-022-16286-0.

[9] T. J. Kwak, H. Jung, B. D. Allen, M. C. Demirel, and W. J. Chang, "Dielectrophoretic separation of randomly shaped protein particles," *Separation and Purification Technology*, vol. 262, May 2021, Art. no. 118280, https://doi.org/10.1016/j.seppur.2020.118280.

[10] A. T. Giduthuri, S. K. Theodossiou, N. R. Schiele, and S. K. Srivastava, "Dielectrophoresis as a tool for electrophysiological characterization of stem cells," *Biophysics Reviews*, vol. 1, no. 1, Dec. 2020, Art. no. 011304, https://doi.org/10.1063/5.0025056.

[11] P. Han *et al.*, "Continuous Label-Free Electronic Discrimination of T Cells by Activation State," *ACS Nano*, vol. 14, no. 7, pp. 8646–8657, Jul. 2020, https://doi.org/10.1021/acsnano.0c03018.

[12] A. Sanchis, M. Sancho, and R. Pethig, "Dielectrophoresis and Theoretical Studies of Dipolar Chaining Effects in Cells," in *2005 IEEE Engineering in Medicine and Biology 27th Annual Conference*, Shanghai, China, Jan. 2006, pp. 4866–4869, https://doi.org/10.1109/IEMBS.2005.1615562.

[13] M. P. Hughes, "Fifty years of dielectrophoretic cell separation technology," *Biomicrofluidics*, vol. 10, no. 3, Jun. 2016, Art. no. 032801, https://doi.org/10.1063/1.4954841.

[14] J. Ding, R. M. Lawrence, P. V. Jones, B. G. Hogue, and M. A. Hayes, "Concentration of Sindbis virus with optimized gradient insulator-based dielectrophoresis," *Analyst*, vol. 141, no. 6, pp. 1997–2008, Mar. 2016, https://doi.org/10.1039/C5AN02430G.

[15] Y. Qiang, J. Liu, F. Yang, D. Dieujuste, and E. Du, "Modeling erythrocyte electrodeformation in response to amplitude modulated electric waveforms," *Scientific Reports*, vol. 8, no. 1, Jul. 2018, Art. no. 10224, https://doi.org/10.1038/s41598-018-28503-w.

[16] C.-F. Chou *et al.*, "Electrodeless Dielectrophoresis of Single- and Double-Stranded DNA," *Biophysical Journal*, vol. 83, no. 4, pp. 2170–2179, Oct. 2002, https://doi.org/10.1016/S0006-3495(02)73977-5.

[17] Y. H. Su, C. A. Warren, R. L. Guerrant, and N. S. Swami, "Dielectrophoretic Monitoring and Interstrain Separation of Intact Clostridium difficile Based on Their S(Surface)-Layers," *Analytical Chemistry*, vol. 86, no. 21, pp. 10855–10863, Nov. 2014, https://doi.org/10.1021/ac5029837.

[18] B. Yafouz, N. A. Kadri, and F. Ibrahim, "Dielectrophoretic Manipulation and Separation of Microparticles Using Microarray Dot Electrodes," *Sensors*, vol. 14, no. 4, pp. 6356–6369, Apr. 2014, https://doi.org/10.3390/s140406356.

[19] R. Natu and R. Martinez-Duarte, "Numerical Model of Streaming DEP for Stem Cell Sorting," *Micromachines*, vol. 7, no. 12, Dec. 2016, Art. no. 217, https://doi.org/10.3390/mi7120217.

[20] E. O. Adekanmbi and S. K. Srivastava, "Dielectrophoretic applications for disease diagnostics using lab-on-a-chip platforms," *Lab on a Chip*, vol. 16, no. 12, pp. 2148–2167, Jun. 2016, https://doi.org/10.1039/C6LC00355A.

[21] F. Yang, X. Yang, H. Jiang, W. M. Butler, and G. Wang, "Dielectrophoretic Separation of Prostate Cancer Cells," *Technology in Cancer Research & Treatment*, vol. 12, no. 1, pp. 61–70, Feb. 2013, https://doi.org/10.7785/tcrt.2012.500275.

[22] Y. Wang, X. Ding, and Z. Zhang, "Numerical Study on Separation of Circulating Tumor Cell Using Dielectrophoresis in a Four-Electrode Microfluidic Device," *Journal of Shanghai Jiaotong University (Science)*, vol. 28, no. 4, pp. 391–400, Aug. 2023, https://doi.org/10.1007/s12204-022-2459-9.

[23] N. V. Nguyen, H. Van Manh, and N. Van Hieu, "Numerical simulation-based performance improvement of the separation of circulating tumor cells from bloodstream in a microfluidic platform by dielectrophoresis," *Korea-Australia Rheology Journal*, vol. 34, no. 4, pp. 335–347, Nov. 2022, https://doi.org/10.1007/s13367-022-00039-6.

[24] S. Ganesan and A. V. Juliet, "Computational analysis on design and optimization of microfluidic channel for the separation of Staphylococcus aureus from blood using dielectrophoresis," *Journal of the Brazilian Society of Mechanical Sciences and Engineering*, vol. 45, no. 12, Nov. 2023, Art. no. 624, https://doi.org/10.1007/s40430-023-04523-0.

[25] S. Tomescu and I. O. Bucur, "Numerical Investigation of Oil Gas Separation with the Use of VOF CFD," *Engineering, Technology & Applied Science Research*, vol. 11, no. 6, pp. 7841–7845, Dec. 2021, https://doi.org/10.48084/etasr.4446.

[26] M. Elitas *et al.*, "Dielectrophoresis as a single cell characterization method for bacteria*," *Biomedical Physics & Engineering Express*, vol.

3, no. 1, Jan. 2017, Art. no. 015005, https://doi.org/10.1088/2057-1976/3/1/015005.

[27] A. K. M. F. K. Rasel, S. L. Seyler, and M. A. Hayes, "A numerical study on microfluidic devices to maintain the concentration and purity of dielectrophoresis-induced separated fractions of analyte," *Analytical and Bioanalytical Chemistry*, vol. 415, no. 20, pp. 4861–4873, Aug. 2023, https://doi.org/10.1007/s00216-023-04795-4.

[28] C. L. Kumar, A. V. Juliet, B. Ramakrishna, S. Chakraborty, A. M. Mazin, and A. S. Kalakanda, "Computational Microfluidic Channel for Separation of Escherichia coli from Blood-Cells," *Computers, Materials & Continua*, vol. 67, no. 2, pp. 1369–1384, 2021, https://doi.org/10.32604/cmc.2021.015116.